Colloid Polym Sci (2011) 289:569–581
DOI 10.1007/s00396-011-2384-1

ORIGINAL CONTRIBUTION

Collapse transition in thin films of poly(methoxydiethylenglycol acrylate)

Qi Zhong · Weinan Wang · Joseph Adelsberger · Anastasia Golosova · Achille M. Bivigou Koumba · Andre Laschewsky · Sergio S. Funari · Jan Perlich · Stephan V. Roth · Christine M. Papadakis · Peter Müller-Buschbaum

Received: 14 October 2010 / Revised: 14 January 2011 / Accepted: 16 January 2011 / Published online: 12 February 2011

Abstract The thermal behavior of poly(methoxydiethylenglycol acrylate) (PMDEGA) is studied in thin hydrogel films on solid supports and is compared with the behavior in aqueous solution. The PMDEGA hydrogel film thickness is varied from 2 to 422 nm. Initially, these films are homogenous, as measured with optical microscopy, atomic force microscopy, X-ray reflectivity, and grazing-incidence small-angle X-ray scattering (GISAXS). However, they tend to de-wet when stored under ambient conditions. Along the surface normal, no long-ranged correlations between substrate and film surface are detected with GISAXS, due to the high mobility of the polymer at room temperature. The swelling of the hydrogel films as a function of the water vapor pressure and the temperature are probed for saturated water vapor pressures between 2,380 and 3,170 Pa. While the swelling capability is found to increase with water vapor pressure, swelling in dependence on the temperature revealed a collapse phase transition of a lower critical solution temperature type. The transition temperature decreases from 40.6 °C to 36.6 °C with increasing film thickness, but is independent of the thickness for very thin films below a thickness of 40 nm. The observed transition temperature range compares well with the cloud points observed in dilute (0.1 wt.%) and semi-dilute (5 wt.%) solution which decrease from 45 °C to 39 °C with increasing concentration.

Keywords Hydrogel · Thin film · Thermoresponsive · LCST behavior · GISAXS · AFM

Q. Zhong · W. Wang · J. Adelsberger · A. Golosova · C. M. Papadakis · P. Müller-Buschbaum (✉)
Physikdepartment, Lehrstuhl für Funktionelle Materialien,
Technische Universität München,
James-Franck-Str. 1,
85747 Garching, Germany
e-mail: muellerb@ph.tum.de

A. M. Bivigou Koumba · A. Laschewsky
Institut für Chemie, Universität Potsdam,
Karl-Liebknecht-Str. 24-25,
14476 Potsdam-Golm, Germany

S. S. Funari · J. Perlich · S. V. Roth
HASYLAB at DESY,
Notkestr. 85,
22603 Hamburg, Germany

Introduction

Thermoresponsive polymers have attracted considerable attention due to the manifold applications which arise from the ability to switch such material by a change in temperature. Examples of applications are valves in micro-fluidics, thermosensitive surfaces, artificial pumps and muscles, light modulation systems, optical switches, and the release of drugs in the body or sensors. When a strong change of volume is desired even for small changes of temperature, the collapse transition of polymers with a lower critical solution temperature (LCST) behavior is well suited to install such thermoresponsive behavior. Currently, the most frequently studied polymer with LCST behavior is poly(*N*-isopropylacrylamide) (PNIPAM) [1]. It exhibits an LCST of about 32 °C that is attributed to alterations in the hydrogen-bonding interactions of the secondary amide group [1–5]. In addition to extensive bulk investigations on PNIPAM solutions [6–8], PNIPAM gels [9–14], and recently PNIPAM-based thin films have been investigated [15–24]. Significant macroscopic volume changes were obtained, and the switchability of thin films was reported.

The LCST of PNIPAM in water is slightly lower than body temperature and thus has promoted interest in

biomedical applications [25–27]. This value however imposes limitations to applications which aim at higher temperatures. Therefore, alternative thermoresponsive systems with an LCST well above 32 °C are desirable. Moreover, from a fundamental point of view, it is interesting to extend the investigations concerning LCST behavior of non-ionic polymers in aqueous systems to polymers, which do not bear a "self-consisting" secondary amide group (as in PNIPAM) that is able to participate as a donor as well as an acceptor in hydrogen bonding. In this respect, oligoethylenglycol-based polymers, in particular, acrylates and methacrylates, are an attractive class of polymers exhibiting a LCST behavior [28]. Their phase transition temperature (PTT) can easily be adjusted via the number of ethyleneglycol repeat units. Thus, we have been interested in investigating the polymer of methoxydiethyleneglycol acrylate (MDEGA), denoted poly(methoxydiethylenglycol acrylate) (PMDEGA), as such a thermoresponsive model polymer, which exhibits a PTT in the range of about 40 °C [29].

We focus on solutions as well as on thin films and address the film stability and the LCST-type behavior. Among the large variety of different thin film preparation techniques, the grafting approach [30–35] and the spin-coating technique [16–18, 36] are most widely used in the preparation of thermoresponsive surfaces and thin films. Spin-coating has proven to be particularly useful [16–18], being widely applicable in many areas of thin polymer films and offering the possibility to control the film thickness over a large range.

Our structural investigations of thin films are based on scattering techniques, such as X-ray reflectivity and grazing-incidence small-angle X-ray scattering (GISAXS) and are complemented by optical and atomic force microscopies. Thus, the surface and the inner film structure can be accessed. The LCST-type behavior for the thin PMDEGA hydrogel films is probed in swelling experiments in water vapor atmosphere. It is compared with the PTT of PMDEGA in bulk solution samples as probed with turbidimetry and small-angle X-ray scattering (SAXS).

Experimental section

Materials

Carbon disulfide [75-15-0] (99.9%, Acros Organics), propanethiol [2107-03-9] (99%, Sigma-Aldrich), 4-methoxybenzylbromide [2746-25-0] (with 3 w.% K_2CO_3, Sigma-Aldrich), dichloromethane [75-09-2] (Acros Organics), $CHCl_3$ [37-297-8] (99%, Sigma-Aldrich), triethylamine [121-44-8] (99%, Acros Organics), basic Al_2O_3 (Acros Organics, activated, 50-200 micron), and magnesium sulfate [7487-88-9] (97%, Acros Organics) were used as received. Tetrahydrofuran (THF) was distilled over K–Na. Azoisobutyronitrile (AIBN; Wako) was recrystallized from methanol. Regenerated cellulose dialysis tubing [Zellu Trans 3,5, Roth (Germany)] had a nominal cut-off of 4.000–6.000 g/mol. Monomer methoxydiethyleneglycol acrylate (MDEGA) was synthesized according to the literature [29].

Synthesis of RAFT agent CTA and polymer

The chain transfer agent 4-methoxybenzylsulfanylthiocarbonylsulfanylpropane (CTA) was synthesized in 90% yield from propanethiol, carbon disulfide, and 4-methoxybenzylbromide in CH_2Cl_2 with triethylamine as auxiliary base, adapting a standard procedure [37].

Elemental analysis: ($C_{12}H_{16}OS_3$, M_r=272.46): Calc. C 52.90%, H 5.92%, S 35.31%; found: C 53.13%, H 5.90%, S 34.63 %.

MS (EI, negative ions): m/z=272.45. EA

^{1}H-NMR (300 MHz in $CDCl_3$, δ in parts per million [ppm]): δ=1.12 (*t*, 3H, CH_3-), 1.83 (*m*, 2HS-C-CH_2-), 3.45 (*t*, 4 H, S-CH_2-), 3.88 (*s*, 3 H, CH_3O-), 4.66 (*s*, 2 H, CH_2-aryl), 6.93 (*d*, 2 H, -CH=C-O-), 7.34 (*d*, 2 H, =CH-C=C-O-). ^{13}C-NMR (75 MHz in $CDCl_3$, δ in ppm): δ=13.41 ($\underline{C}H_3$-), 21.50 (CH_3-$\underline{C}H_2$-), 38.72 (-S-$\underline{C}H_2$-alkyl), 40.92 (-S-$\underline{C}H_2$-aryl), 114.05 (-$\underline{C}$H=C-O aryl), 126.60 (=$\underline{C}$< aryl), 130.38 (=$\underline{C}$H-C=C-O aryl), 159.12 (=$\underline{C}$-O aryl), 223.90 (-S-(-($\underline{C}$=S)-S-). UV-vis (in CH_2Cl_2): bands at λ_{max1}= 310 nm (π-π*, ε=16,100 L mol^{-1} cm^{-1}), λ_{max2}=433 nm (n-π*, ε=62.5 L mol^{-1} cm^{-1}).

For polymerization, monomer MDEGA (5.0 g; 8.7 mmol) and RAFT agent CTA (0.0686 g; 0.25 mmol) were dissolved in toluene (8 mL). AIBN (0.0082 g; 0.050 mmol) in THF (2 mL) was added, and the mixture was purged with argon for 15 min. The sealed reaction flask was immersed into an oil bath preheated to 70 °C. After 6 h, the reaction was quenched by placing the flask into liquid nitrogen. The mixture was diluted with acetone and precipitated thrice into hexane (300 mL). The polymer obtained was a hygroscopic, viscous yellow oil, yielding 3.6 g (72%).

The theoretically expected molar mass was M_n^{theo}= 14,700 g/mol, and the apparent molar mass according to SEC was M_n^{app}=9,700 g/mol (based on polystyrene standards) with a polydispersity index PDI of 1.7. End-group analysis by ^{1}H-NMR spectroscopy via the initiating R-group compared the integrals of the aryl proton signals at 6.9 and 7.3 ppm with the integral of the signal of the ester α-methylene protons of the constitutional repeat unit at 4.2 ppm and gave a number average molar mass of M_n= 17,000 g/mol. Though less reliable as full conservation of the active Z end-groups must be assumed, end-group analysis can be performed alternatively on the basis of the active chain end Z-groups, quantifying the content of the thiocarbonyl chromophore by UV-vis spectroscopy (in CH_2Cl_2, using the

extinction coefficient of 16100 L mol^{-1} cm^{-1} at 310 nm of the RAFT agent engaged). Thus, a number average molar mass of M_n^Z=24,000 g/mol is formally calculated.

Substrate cleaning and thin film preparation

Silicon (Si) with a thin oxide layer surface was used as the substrate. The precut Si was placed in dichloromethane at 46 °C for 30 min and rinsed with Millipore water shortly. Afterward, the Si was placed into a base solution containing 350 mL water, 30 mL H_2O_2, and 30 mL NH_3 at 76 °C for 2 h to clean the substrates and remove organic traces. Then, the Si was stored in Millipore water. Before spin-coating of the PMDEGA solution, the Si was rinsed with Millipore water to remove any possible trace of the basic bath. Compressed nitrogen was used to dry the Si substrate. Because of this cleaning protocol, a hydrophilic oxide layer of 5 nm was present at the Si surface [38].

Dry PMDEGA films were prepared by spin-coating (2,000 rpm, 30 s) from 1,4-dioxane at room temperature (relative humidity 40%) onto the pre-cleaned Si substrates. The concentration of the PMDEGA solution varied from 1 to 60 mg/mL to obtain different PMDEGA film thicknesses. The solutions used for spin-coating were transparent and did not show any sign of aggregates. Several identical samples were prepared to prove the reproducibility.

Methods

Spectroscopy

NMR spectra were taken with an apparatus Bruker Avance 300 (300 MHz). Mass spectra were recorded by a GC/MS-system Trace DSQII (Thermo Scientific). Elemental analyses were carried out using a Vario ELIII microanalyzer (Elementar Analysensysteme, Germany). UV-vis spectra were recorded on a spectrophotometer Cary-1 (Varian) using quartz cuvettes (Suprasil, Hellma, Germany, optical path length 10 mm).

Thermal analysis

Thermal properties of the polymers were characterized by thermogravimetry (TGA) with an apparatus TGA/SDTA 851 (Mettler Toledo) and by differential scanning calorimetry (DSC) with a model DSC 822 differential scanning calorimeter (Mettler Toledo) under nitrogen atmosphere, applying heating and cooling rate of 20 K/min.

Size-exclusion chromatography

Size-exclusion chromatography (SEC) of the polymers was run in *N*,*N*-dimethylacetamide containing 0.1 % LiBr as eluent at a column temperature of 45 °C, with a setup consisting of an Agilent 1200 isocratic pump, an Agilent 1200 refractive index detector, and two GRAM columns (10 μm, 8×300 mm, pore sizes 100 and 1,000; PSS GmbH, Mainz, Germany). The SEC setup was calibrated using low polydispersity polystyrene standards (PSS GmbH, Mainz, Germany).

Turbidimetry

Turbidity measurements were performed on a temperature-controlled turbidimeter (model TP1, E. Tepper, Germany) with heating and cooling rates of 1.0 K/min, respectively. The transmittance of the polymer solutions was set automatically to 100% at the beginning of each measurement. Temperatures are precise within 0.5 K.

For cloud point determination, polymer samples were directly dissolved in water with a concentration of 1 mg/mL. The cloud points of the aqueous solutions were measured by turbidimetry at a fixed heating/cooling rate of 1 °C/min. The temperature at which the first deviation of the scattered light intensity from the baseline of the turbidity curve occurred was taken as the cloud point.

Dynamic light scattering

Dynamic light scattering (DLS) was carried out using a high-performance particle-sizer (HPPS-ET, Malvern Instruments, UK) equipped with a He–Ne laser (λ=633 nm) and a thermoelectric Peltier temperature controller. Polymers were directly dissolved at ambient temperature in deionized water with a concentration of 1.0 mg/mL. The measurements were made at the scattering angle of θ=173° ("backscattering detection"), and the autocorrelation functions were analyzed with the CONTIN method.

Small-angle X-ray scattering

SAXS experiments were performed at beamline A2, HASYLAB at DESY in Hamburg, Germany. An X-ray beam with a wavelength λ=0.15 nm and a size of 2×3 mm was used. The detector was a MarCCD camera with a resolution of 1,024×1,024 pixels, which was mounted 1.0387 m from the sample. A piece of lead was used as the beam stop. The accessible q-range with this setup was 0.25–3.4 nm^{-1}. The background was determined using D_2O. The q calibration was performed using silver behenate.

The polymer was dissolved in D_2O at a polymer concentration c = 50 mg/mL and was stored in the fridge 2 days prior to the SAXS experiment. The polymer solution was mounted between two pieces of Kapton foil in a sample holder with five sample positions. The temperature was controlled by a JUMO temperature controller and was measured by a thermocouple directly embedded in one of the sample cells. The sample thickness was 2 mm.

Measurements were carried out between 27 °C and 55 °C. Each measurement took 200 s with waiting times of 10 min after each change of temperature.

For the analysis of the SAXS curves, the NIST SANS package 7.02 implemented in the software IGOR Pro 6.1 was used [39]. The data were fitted with a combined equation following Refs. [11, 40]:

$$I(q) = \frac{I_{OZ}}{\left[1 + \xi^2 q^2 (D+1)/3\right]^{D/2}} + I_g \exp\left(-\frac{R_g q^2}{3}\right) + \frac{K}{q^\alpha} + bg \quad (1)$$

The first term describes the solution-like concentration fluctuations by a generalized Ornstein–Zernike equation (OZ) for a polymer system with a certain fractal dimension, D. ξ is the correlation length of concentration fluctuations, and I_0 a scaling factor. The second term corresponds to solid-like concentration fluctuations and is a function of the radius of gyration R_g of polymer-rich or polymer-poor domains of the solution with a scaling factor I_g. In our case of a relatively dilute solution, we attribute it to polymer-rich domains. It reflects the incomplete hydration of PMDEGA. To describe the increasing scattering observed at small q values, a generalized Porod law is added (third term), which includes the Porod amplitude K and the Porod exponent α. bg denotes the incoherent background.

Optical microscopy and atomic force microscopy

The sample surfaces were observed with optical microscopy using a Zeiss Axiotech 25 H optical microscope with magnifications between ×1.25 and ×50. A PixeLink S621CU CCD camera was used to record the micrographs.

With a PARK Autoprobe CP atomic force microscope, the sample surface was probed at high resolution. All measurements were performed at ambient conditions. Each scanned micrograph consists of 256 lines, scanned with 0.25 up to 1.0 Hz. Several images were measured for each sample. Micrographs were recorded at different sample positions. Contact avoidance to the sample minimized the tip-induced sample degradation. The silicon gold-coated conical cantilevers had resonant frequencies at about f= 80 kHz and a spring constant of approximately 2.3 Nm^{-1}. At each individual sample position, scans with different ranges from 0.5×0.5 μm up to 10×10 μm were performed. From the raw data, the background due to the scanner tube movement was fully subtracted to determine the values of the rms roughness over the complete scan area.

X-ray reflectivity measurements

X-ray reflectivity (XRR) curves were measured with a Siemens D5000 diffractometer using a reflectivity extension. The measurements were performed in air with a scintillation counter. The samples were fixed on the sample stage by vacuum. A tantalum knife edge was mounted above the sample surface to reduce background and to control the footprint of the X-ray beam on the sample. The measurements were performed at a wavelength of λ= 0.154 nm (secondary graphite monochromator, Cu Kα). Data were fitted by the program Parratt32 [41] using the Parratt algorithm [42]. A model with different refractive layers was assumed in the program.

Optical interference measurements

Sample thicknesses and optical properties (i.e., the refractive index, n) were measured with the Filmetrics F20 ThinFilm Measurement System (Filmetrics Inc., San Diego). By adjusting the distance between the sample and the beam cable, the spot size of the light beam varied from 500 μm to 1 cm. The wavelength used for obtaining the characteristic intensity oscillation curve in the measurement was in the region from 400 to 1,100 nm. For the swelling behavior measurements, dry PMDEGA films were placed in a small aluminum chamber under water vapor conditions. The incident beam passed through the glass windows on top of the chamber. Due to interference of the light multiply reflected from the film surface and the film/substrate interface, an interference fringe pattern is observed in the reflected intensity. The positions and amplitudes of the fringes are related to the film thickness and the refractive index, n. By fitting these curves, the thickness and the refractive index of PMDEGA films were obtained.

Grazing-incidence small-angle X-ray scattering measurements

GISAXS measurements were carried out at the beamline BW4 of the DORIS III storage ring at HASYLAB (DESY, Hamburg) [43]. The selected wavelength was λ=0.138 nm. The beam divergence in and out of the plane of reflection was set by two entrance cross-slits. To operate a microbeam the X-ray beam was moderately focused to the size of (H×B) 40×60 μm^2 by using an assembly of refractive beryllium lenses [44]. The sample was placed horizontally on a goniometer. A beam stop was used to block the direct beam in front of the detector (MARCCD; 2,048×2,048 pixels). A second, point-like moveable beam stop was also used to block the specular peak on the detector. The incident angle was set to α_i=0.35° for the initially prepared PMDEGA film, and α_i=0.365° for the PMDEGA film after being exposed to water vapor, which is well above the critical angles of PMDEGA (0.149°) and of Si (0.20°). As a result, specular and Yoneda peak are well separated on the

detector and both, the sample surface and the film are probed [45–48]. At the chosen sample-detector distance of 2.22 m (for the initially prepared PMDEGA film) and 1.99 m (for the PMDEGA film after being exposed to water vapor), the Yoneda and the specular peak are well separated on the detector. Due to the simple shape of the two-dimensional GISAXS pattern, structural information is obtained from vertical and horizontal cuts of the 2D intensity distribution [48–50].

The vertical cut at q_y=0, called detector cut, contains the information of the structure perpendicular to the surface. Horizontal cuts at constant q_z allow extracting the information (geometry, size distribution, and spatial correlation) of lateral structures. The intensity of the q_y-cuts was integrated over a small slice Δq_z in the vertical direction to obtain improved statistics. In literature, these horizontal cuts are also named as GISAXS cuts and out-of-plane cuts [48].

Results and discussion

Synthesis and molecular characterization

Homopolymers PMDEGA were synthesized via radical addition-fragmentation chain transfer (RAFT) polymerization, using the RAFT agent CTA and AIBN as free radical initiator (see Fig. 1). The polymerization proceeded smoothly, to give the polymer in good yield as a highly viscous, tacky mass, in agreement with a glass transition temperature of PMDEGA of about −50 °C [51, 52].

Characterization by SEC in dimethylacetamide reveals a monomodal molar mass distribution, with a moderate polydispersity of 1.7. The obtained apparent number average molar mass of M_n^{app}=9,700 must be taken as approximate only, as polystyrene standards are used for calibration. Fortunately, the ^{1}H-NMR spectrum of PMDEGA exhibits in addition to the characteristic signals of the repeat units also some signals of end groups incorporated via the RAFT agent CTA (see Fig. 2). In particular, the protons of the phenylene end group are resolved (protons "b" and "c"), so that their quantification relative to the signal intensity of a characteristic signal of the constitutional repeat units (such as protons "g") enables to determine an absolute number average molar mass by end-group analysis, to give a molar mass of M_n=17,000 g/mol. This value is in good agreement with the theoretically expected one of M_n^{theo}=14,700 g/mol. The comparison of the data of M_n and M_n^{app} shows that the mismatch is less dramatic in the case of PMDEGA than for higher poly (oligoethyleneglycol acrylate)s [53], but it is still substantial. Additionally, the strong thiocarbonyl chromophore of the Z-group at the active chain end allows performing an alternative end group determination via UV-vis spectroscopy, under the assumption that no end groups get lost in the course of the polymerization reaction. The thus obtained value of M_n^Z=24,000 g/mol is somewhat higher than the M_n value determined via the R-group, pointing to a loss of about 25–30 % of active end groups in the course of the polymerization process. The occurrence of side reactions during the RAFT polymerization is also suggested by the moderate value of 1.7 for the PDI. This is not too surprising, as the polymerization was performed in THF. While being a good solvent for the reagents and the polymer, this cyclic ether was recently shown to be prone to side reactions in the RAFT process [54, 55]. Also, due to the chemical similarity of the cyclic ether structure of THF and the multiple ether moieties in the methoxyethoxyethyl side chains of PMDEGA, one must take into account possible inherent side reactions of the growing polymer chains with the side chains. Nevertheless, the polymer has a monomodal, reasonably narrow mass distribution, and dissolves completely in water.

Collapse transition of PMDEGA

The cloud point of the PMDEGA in dilute aqueous solution (1 mg/mL) was determined by turbidimetry as 45 °C (see Fig. 3), with only a small hysteresis between heating and cooling cycles. This cloud point measured is taken as PTT for the collapse of the polymer. The value found is higher than the value of 38 °C reported in the literature for a more concentrated solution (10 mg/mL) of PMDEGA [29] for a sample prepared via nitroxide-mediated radical polymerization using 1,1,2,2-tetraphenyl-1,2-diphenoxyethane as mediator, with a molar mass of 9,000 g/mol. This difference

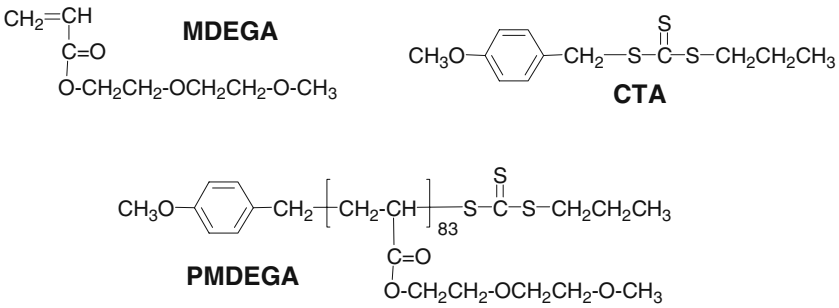

Fig. 1 Chemical formulas of monomer MDEGA, RAFT agent CTA, and polymer PMDEGA used

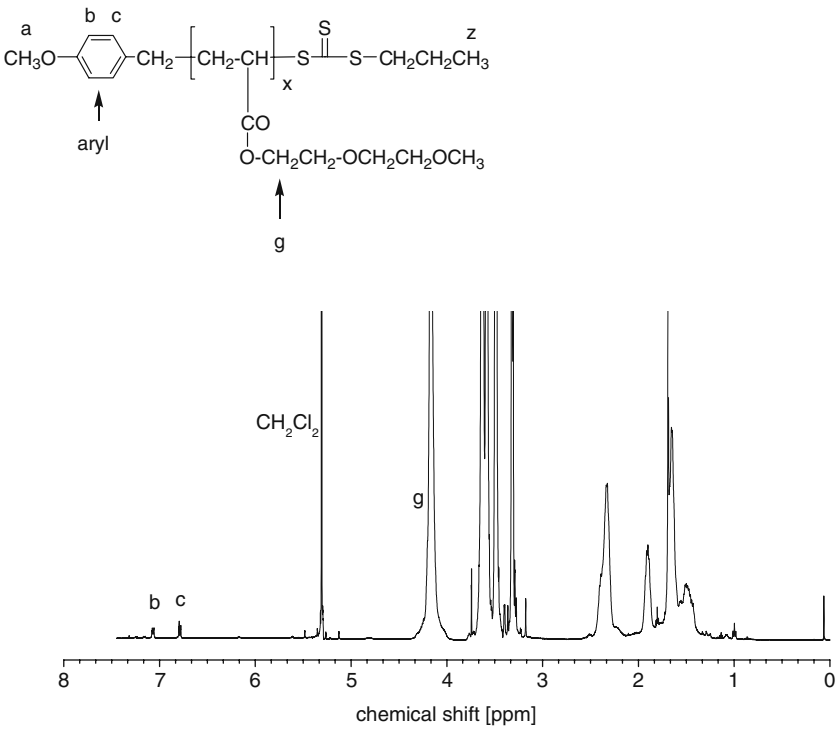

Fig. 2 ^{1}H-NMR spectrum of PMDEGA in CD_2Cl_2

may be explained either by the different concentrations and/or by the different end groups introduced via the different controlling agents, which have been reported to modulate cloud points of a given water-soluble polymer [56–58]. Note that the latter effect is also well known in the case of PNIPAM, whereas the PTT of PNIPAM is nearly independent of the concentration in the range considered [59].

Additional studies by DLS were made to determine the evolution of the hydrodynamic radii upon heating from 20 °C to 60 °C. PMDEGA exists at 20 °C apparently as single polymer coil with a hydrodynamic diameter of 5 nm, while at 60 °C, i.e., well above the cloud point, large aggregates with hydrodynamic diameters of about 700 nm were formed, but no precipitation occurred.

To gain further insights into the collapse transition of PMDEGA, less dilute solutions were investigated with SAXS [60]. In contrast to the turbidity measurements, a higher polymer concentration (50 mg/mL) was chosen to address the semi-dilute regime and to improve the signal. Figure 4 shows representative SAXS scattering curves. Only slight changes are observed in dependence of temperature. At high temperatures, the scattering at low q values is steeper than at high q values, where the scattering also moves towards lower q values with increasing

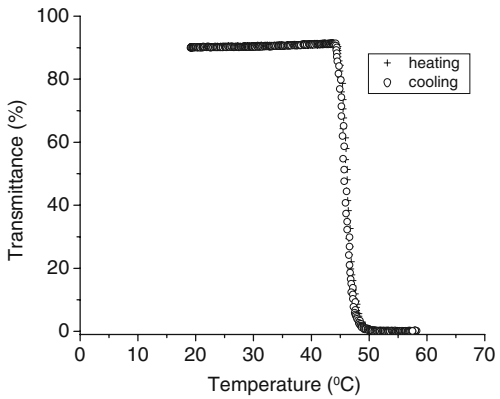

Fig. 3 Temperature-dependent transmittance (I/I_0) of aqueous solution (1 mg/mL) of PMDEGA. Heating and cooling rates are 1 K/min

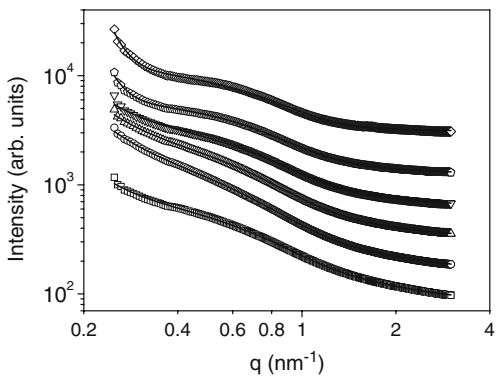

Fig. 4 Scattering curves for 27 °C (*open squares*), 37 °C (*open circles*), 39 °C (*open triangles up*), 41 °C (*open triangles down*), 43 °C (*open pentagons*), and 55 °C (*open diamonds*) together with the fits (*solid lines*). The *curves* are vertically shifted by a factor of 2

temperature. The absence of a discontinuity makes it difficult to identify the PTT directly from the SAXS curves.

The curves could not be fully fitted with a simple OZ law, describing semi-dilute polymer solutions with a correlation length ξ between the polymer strands. The OZ structure factor has to be modified by including a fractal dimension, indicative of the packing of the transient network. We observe two additional features: (1) a decay at intermediate q values and (2) increased forward scattering at $q<\sim 0.5$ nm^{-1} which becomes more pronounced at high temperatures. To describe the scattering at intermediate q values (1), a term describing the scattering from polymer-rich and polymer-poor regions was added to the OZ law. It may be due to incomplete hydration of the PMDEGA chain resulting in a pearl-necklace conformation of the chains [61] or to lumps of only partially dissolved polymer. This contribution includes the radius of gyration of the inhomogeneities, R_g. A generalized Porod law was used to fit the forward scattering (2), describing the scattering of very large particles. Overall, the model chosen describes the curves very well in a wide temperature range.

In the applied fitting, the Porod exponent α was fixed at 4 below the PTT, whereas above the PTT, it was fixed at 6 in order to fit the steep increase in forward scattering. The fractal dimension, D, was fixed at values of 2 and 3 below and above the PTT, respectively, i.e., the classical OZ behavior of polymer solutions is observed below the PTT, whereas the collapsed polymers form a densely packed melt above, in spite of the missing ability to form hydrogen bonds among monomers (in contrast to PNIPAM). Both assumptions result in good fits and do not have an influence on the remaining parameters. In Fig. 5, the fitting results of ξ and R_g are given in dependence on temperature. Below the PTT, ξ increases from 1.29 nm at 27 °C to 2.45 nm at 37 °C, then decreases within 4 K to ~0.7 nm where it stays up to 55 °C. We conclude that the PTT is crossed at (39±2) °C, at a temperature 6 K lower than the one observed in turbidimetry

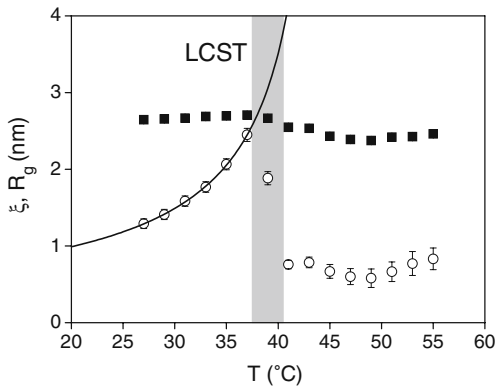

Fig. 5 SAXS results from the fits to the scattering curves. Correlation length ξ (*open circles*) and radius of gyration R_g (*solid squares*). The *full line* is a fit of the scaling law (Eq. 2)

at 1 mg/mL (see above). The PTT thus decreases with increasing concentration, similar to PNIPAM. Fitting a mean-field scaling law [11] to the ξ–values below the PTT:

$$\xi = \frac{\xi_0}{(T_s - T)^v} \tag{2}$$

a spinodal temperature T_s=(45±1) °C and an exponent v= 0.82±0.09 are obtained. The spinodal temperature thus lies above the observed PTT, and the exponent is significantly higher than the value of 0.5 predicted by mean-field theory and observed with PNIPAM [11]. The size of the polymer-rich regions, R_g, is constant at 2.6–2.7 nm below the PTT and decreases gradually to ~2.4–2.5 nm above the PTT. The polymer-rich, presumably, not hydrated domains thus have a size independent on temperature, which only decreases slightly, probably due to the repulsion of even more water.

Structure and stability of PMDEGA films

The combination of the applied base cleaning and spin-coating out of 1,4-dioxane solution enables the preparation of smooth and homogeneous PMDEGA films on Si substrates. Optically and with atomic force microscopy (AFM), no heterogeneities are found in freshly prepared films with thicknesses above 10 nm. Figure 6a shows the PMDEGA film surface of the as prepared film with a thickness of 40 nm as seen with optical microscopy. On a very large surface area, the film is homogeneous. With AFM on a local scale, the film is homogeneous as well (see Fig. 7a). Locally, it has a peak-to-valley surface roughness below 1 nm as determined from the AFM data.

With XRR the film thickness and surface roughness is probed for a significantly larger surface area. Figure 8a shows the measured XRR curves for PMDEGA films of different film thickness together with a fit to the data. In the model, a single PMDEGA layer on top of the Si substrate was assumed. The homogenous polymer layers have the refractive index of PMDEGA. A film thickness regime from 2 to 162 nm is covered in this investigation. In general, within the applied fitting model, the data are well described by the fits. The intensity modulation (Kiessig fringes) in the data of the thinnest PMDEGA film (2 nm) is damped, due to imperfections of the PMDEGA layer. Instead of a continuous and homogenous layer of PMDEGA on the substrate, the PMDEGA forms islands on the substrate, because a very low concentration of PMDEGA in 1,4-dioxane was used to achieve such thin film. The PMDEGA islands cause a large surface roughness and result in damped fringes in the XRR data. At higher PMDEGA concentrations, continuous films are obtained on Si out of 1,4-dioxane solutions. In the XRR curves, the intensity modulations are well pronounced, due to a small

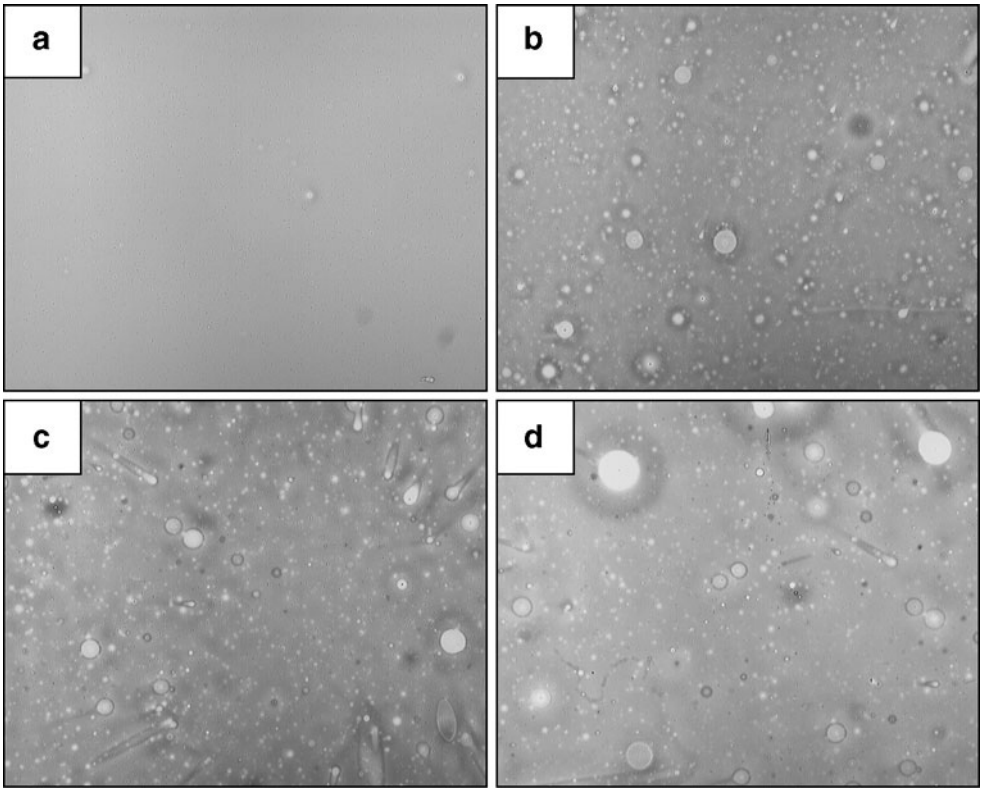

Fig. 6 Optical micrographs of **a** initially prepared PMDEGA (40 nm thickness), **b** after 1, **c** 2, and **d** 6 days storage in air under ambient condition. The micrographs are measured with a magnification of 2.5 and show an area of 4,096×3,276.8 μm^2

surface roughness of the PMDEGA films. The rms-surface roughness values increase with increasing film thickness (see Fig. 8c), however, all values are on the order of 1–2 nm, which matches with AFM observations. Note that the island surface roughness for the thinnest film is not shown in Fig. 8c.

The resulting film thicknesses are shown in Fig. 8b as a function of PMDEGA concentration in the 1,4-dioxane solutions used for spin-coating. It was found empirically for the model system of polystyrene spin-coated from toluene solution that the film thickness increases linearly with the polymer concentration [62]. The same linear concentration dependence matches the PMDEGA films spin-coated out of a 1,4-dioxane solution, as shown by the solid line matching the data points in Fig. 8b. We conclude that, in the addressed concentration regime used to prepare PMDEGA films, the overlap concentration is not reached. The PMDEGA solutions behave like simple homopolymer solutions in the spin-coating process.

All XRR measurements were performed on freshly prepared PMDEGA films. During storage under ambient conditions, the films roughen as illustrated with optical micrographs and AFM. As an example for this aging, optical images of a film with a thickness of 40 nm are shown in Fig. 6 for different storage times. For other PMDEGA film thicknesses, a similar behavior is seen. Whereas the initially prepared film is optically homogeneous with only a very few distortions (here shown to illustrate that the polymer surface is in the focal plane of the optical microscope), an onset of de-wetting is visible already after 1 day (see Fig. 6b). Very clearly, holes of different diameter are seen in the polymer film. Between

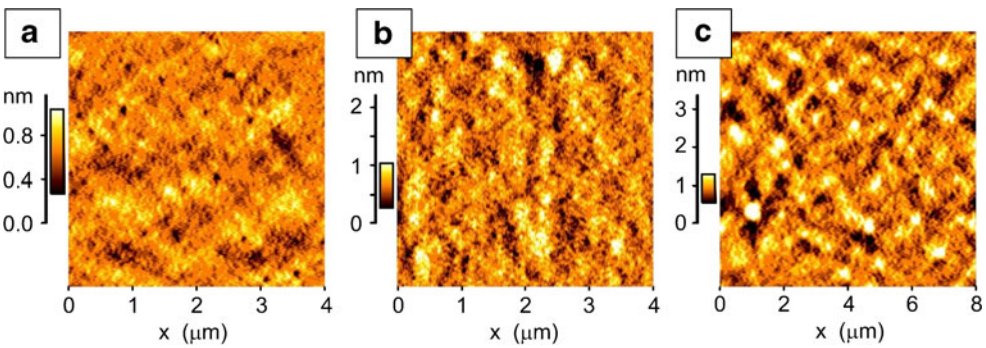

Fig. 7 AFM micrographs of **a** initially prepared PMDEGA (40 nm thickness), **b** after swelling in water vapor, and **c** after 6 days storage in air under ambient condition (measured on a homogeneous spot). The color code for the heights is individually adapted to emphasize on the surface morphology

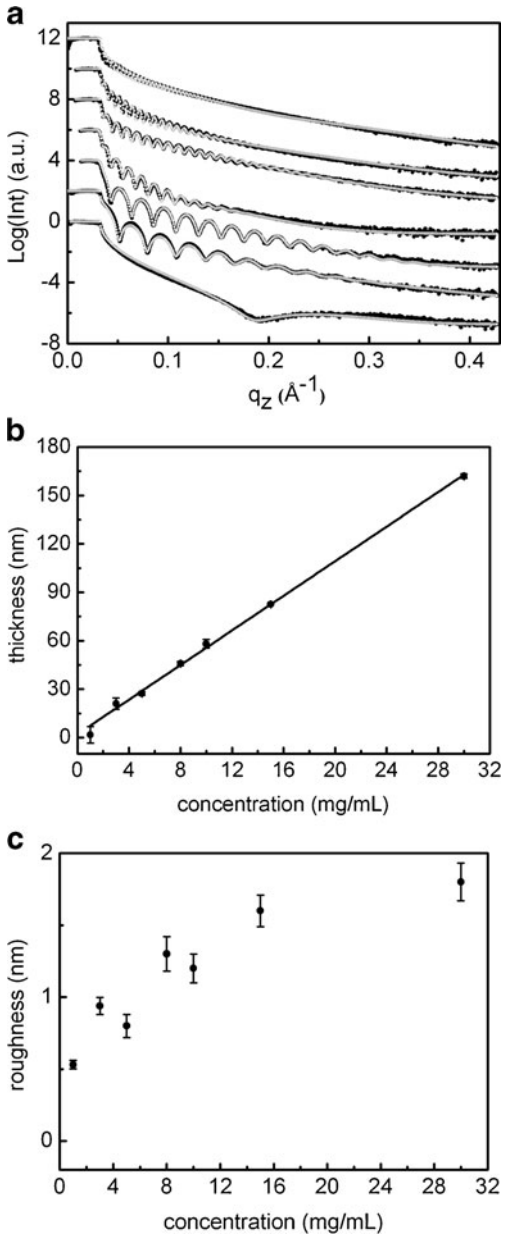

Fig. 8 **a** Representative X-ray reflectivity curves (*dots*) shown together with model fits (*lines*) for the thickness regime covered in this investigation. With increasing film thickness (2, 21, 27, 46, 58, 83, and 162 nm from *bottom* to *top*), the *curves* are shifted along the *Y*-axis for clarity of the presentation. **b** Film thickness, **c** surface roughness plotted as a function of the PMDEGA concentration of the 1,4-dioxane solution used for spin-coating. The *solid line* is a linear fit

the holes, a still-homogeneous PMDEGA film is present, which however is increased in its surface roughness as well (see AFM image in Fig. 7c). The broad distribution of hole diameters indicates a nucleated de-wetting process with grains of different nucleation strength being embedded in the PMDEGA film and acting as nucleation sites. Such grains might be partially dissolved polymer as observed in the SAXS measurements described above, although a better solubility of PMDEGA in 1,4-dioxane is to be expected. Impurities such as dust particles can be excluded due to applied filtering of the solutions used for spin-coating. The holes grow with time and a further roughening of the film occurs (see Fig. 6c, d); however, a complete destruction into isolated polymer drops is not found. Thus, the PMDEGA films are not unstable on the base-treated Si surfaces, but are metastable and only partially destroyed in the areas influenced by the non-swollen nucleation sites [63].

A corresponding de-wetting behavior was not observed in the PNIPAM-based thermoresponsive films [16–18] on identically treated Si surfaces. At first glance, this might be caused by the strong differences in the glass transition temperatures T_g (PMDEGA well below RT with T_g=−50 °C [52] and PNIPAM well above RT with T_g=142 °C), resulting in a significantly different mobility of the polymer chains at room temperature. However, in thin films, the interaction of the solid support has a strong influence of the glass transition temperature which may be very different from the bulk. For example, T_g values of poly(methyl methacrylate) films on substrates of SiO_x and on SiO_x coated with hexadecyltrimethoxysilane are increased or decreased, respectively [64]. As a consequence, PMDEGA chains have a sufficiently high mobility on base-treated Si, whereas PNIPAM chains do not have this mobility.

To deepen this question, the long-ranged correlation in thin PMDEGA films is investigated. Using GISAXS, these correlations along the surface normal can be probed [65–67]. In case the chains are close to immobile in the thin polymer film, a roughness correlation between the solid support and the polymer surface is installed by spin-coating. In many glassy polymers, this correlated roughness has been found [67]. Being energetically unfavorable for the polymer chain, this correlation is cured if the polymer is sufficiently mobile. In a GISAXS measurement, correlated roughness causes intensity modulations along the vertical direction (q_z axis) due to partial phase coherence of diffusely scattered waves [65].

In Fig. 9, the example of a PMDEGA film with 40 nm film thickness is addressed. The corresponding GISAXS data are shown together with vertical cuts. Results from the initially prepared film are compared with results from a film exposed to water vapor atmosphere. Obviously, the vertical cuts exhibit no modulations in the intensity, and only the Yoneda and specular peak are present, even though the resolution of the setup is highly sufficient to resolve possible modulations. Thus, already, the initially prepared PMDEGA film has sufficient mobility to cure the long-ranged correlation, and no correlated roughness is found in PMDEGA. In contrast, in PNIPAM films strong intensity modulations were observed [16], which proves that the PNIPAM films are glassy and frozen-in after spin-coating.

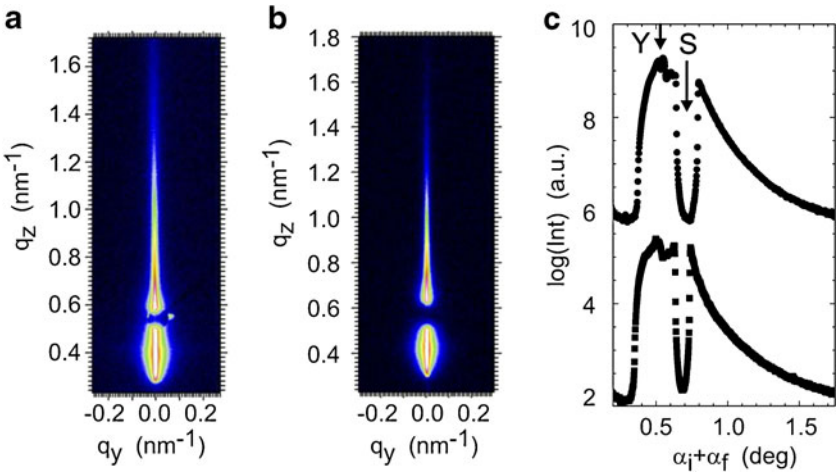

Fig. 9 GISAXS data of a 40 nm thick PMDEGA film: **a** two-dimensional images of the initially prepared film and **b** of the film after exposure to water vapor. **c** Vertical cuts from these two-dimensional data at q_y=0 with Yoneda and specular peak indicated (initially prepared at bottom and water vapor exposed top curve)

Removing the PMDEGA films from ambient conditions by placing them in a desiccator is a way to improve film stability. Optical microscopy showed that films stored in dry conditions remain homogeneous for 4 days, and de-wetting occurred only after 6 days. Thus, the de-wetting is retarded compared with the films stored in ambient conditions (1 day). We conclude that the humidity at room temperature under ambient conditions is sufficient to make the PMDEGA films swell. Incorporation of water from the surrounding air causes a plastification of the PMDEGA films and thus further increases the chain mobility.

Swelling and collapse transition of PMDEGA films

The swelling capability of thin PMDEGA films was investigated in optical interference measurements. The PMDEGA films were placed in a sealed chamber which contained a water reservoir to install saturation conditions. The swelling behavior of PMDEGA films at room temperature is shown in Fig. 10a for the example of a film thickness of 42 nm. The relative change in film thickness is monitored as a function of time. Freshly prepared PMDEGA films were exposed to different water vapor pressures created by aqueous sodium chloride solutions with different concentrations. Thus, the swelling in different water vapor pressures is probed in this experiment. From the top to the bottom, the concentration of sodium chloride solution increases from 0 to 0.36 g/mL, which corresponds to a saturated water vapor pressure decrease from 3,169 Pa (0 g/mL) to 2,380 Pa (0.36 g/mL). At 3,169 Pa, the strongest swelling is probed. Equilibrium is reached after 60 min. After this exposure time, films are still homogeneous but slightly roughened as probed with AFM (see Fig. 7b). The peak-to-valley surface roughness increases to values above 1 nm. For exposure times longer than ~70 min, the swollen film undergoes instability, and de-wetting sets in. In the optical interference measurement, the de-wetting appears as a further increase in film thickness due to film heterogeneities. Because the PMDEGA film has already incorporated water during the initial swelling, the polymer chain mobility is further enhanced as compared with the initially prepared films. As a consequence, the de-wetting process happening in

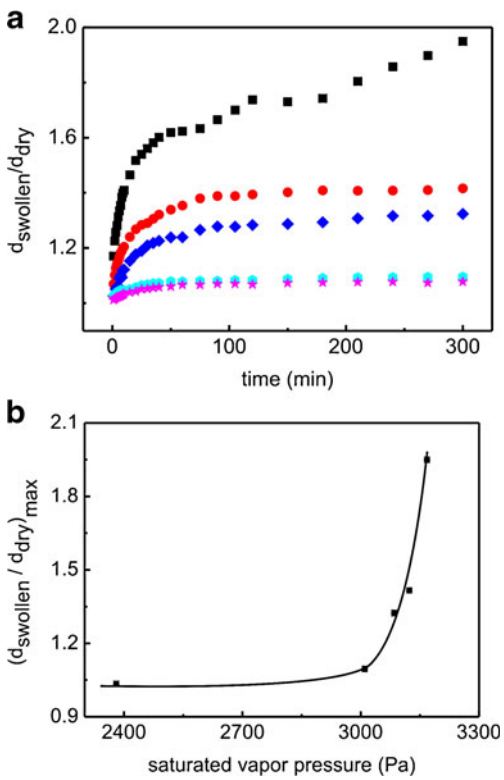

Fig. 10 **a** Swelling behavior of PMDEGA films when exposed to sodium chloride solutions with different concentrations. From *top to bottom*, the concentrations of the sodium chloride solution are 0 (*squares*), 0.045 (*circles*), 0.09 (*rhombs*), 0.18 (*hexagons*), 0.36 g/mL (*stars*). **b** Ratio of the maximal reached swollen PMDEGA film thickness normalized to the initial dry film thickness as a function of the vapor pressure. The *solid line* is a guide to the eye

the dry film under ambient conditions in days is accelerated to hours in the swollen film.

With decreasing value of the saturated vapor pressure, the ability of the films to swell also decreases, and the tendency of the films to de-wet is less pronounced. The swelling capability of the investigated PMDEGA films is sensitive to the surrounding vapor pressure. Figure 10b summarizes this behavior in plotting the swelling capacity (swollen film thickness normalized to the initial dry film thickness of the respective PMDEGA film) as a function of the vapor pressure. The film thickness of the swollen PMDEGA film depends on the water vapor pressure in a strongly non-linear way. At low water vapor pressure, there are not sufficient water molecules present in the surrounding of the PMDEGA film to saturate all monomers and to reach the full swelling capacity.

To address the collapse transition, the temperature-dependence of the film thickness is measured. Starting at 31 °C, which is below the PTT known from the bulk investigations, the freshly prepared PMDEGA film is exposed to water vapor atmosphere installed at a fixed salt concentration in the water reservoir of the chamber. The measured changes in the film thickness are shown in Fig. 11a for three different vapor pressures (installed by three sodium chloride solution with different concentrations). Figure 11 compares samples with an equal initial film thickness of 42 nm. At a concentration of the sodium chloride solution of 0.023 mg/mL (squares in Fig. 11a), the PMDEGA film shows the strongest response, with the largest change in film thickness due to the chain collapse. The higher sodium chloride concentrations 0.045 and 0.09 mg/mL result in a weaker shrinkage and in a shift of the PTT to slightly higher temperatures. Thus, the decrease of saturated vapor pressure causes the transition temperature to shift to higher temperature, while the transition becomes broader as is more clearly seen from the first derivatives shown in Fig. 11b.

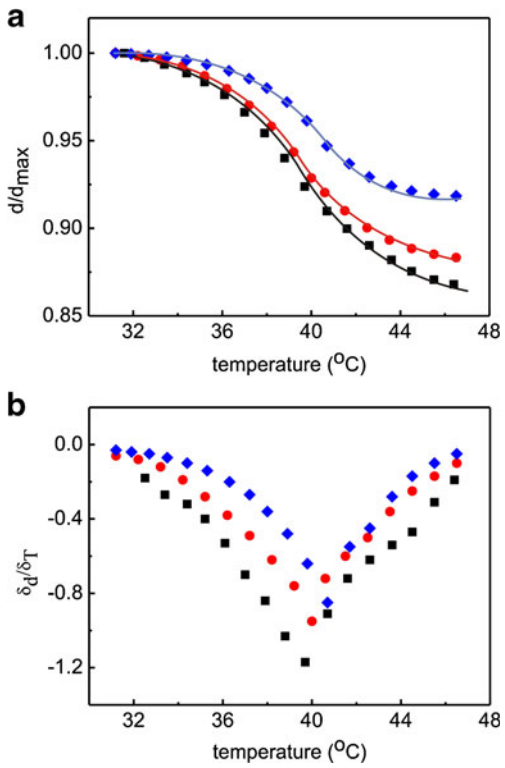

Fig. 11 **a** Temperature-dependent changes of the film thickness measured for PMDEGA films when exposed to sodium chloride solution with different concentration of 0.023 mg/mL (*squares*), 0.045 mg/mL (*circles*), and 0.09 mg/mL (*rhombs*). The *solid lines* are guides to the eye. **b** Corresponding first derivatives of these data

In general, all transitions appear broader as compared with the behavior measured for PNIPAM-based films. This increased width of the transition region matches with the observations in semi-dilute solutions as probed with SAXS. This phenomenon is not limited to a selected film thickness, as Fig. 12 demonstrates. At a fixed value of the sodium chloride solution concentration (0.045 g/mL), the film thickness dependence of the PTT is determined. For film thicknesses between 17.4 and 422.6 nm, a broad transition is seen.

Similar to the behavior of PNIPAM films, the strength of the chain collapse depends on the film thickness. The thinner the PMDEGA film, the stronger is the probed response to the temperature change and the change in film thickness caused by the chain collapse. The thin film (thickness 17.4 nm) reduces its thickness by more than 20 % when passing the PTT, whereas the thick film (thickness 422.6 nm) shrinks only by 7% (see Fig. 12a). Moreover, the transition temperature decreases slightly with increasing film thickness (see Fig. 12b). The thickness-dependent change of the transition temperature is illustrated in Fig. 12c. In the thin film regime (up to film thicknesses of 40 nm), a plateau is present, which means that, in this region, an increase in the film thickness does not cause a change of the transition temperature. Above this critical film thickness, a further increase of the film thickness affects the PTT, and a decrease from 40.6 °C (41.1 nm) to 36.6 °C (422.6 nm) is detected.

In literature, only few swelling experiments with thin PNIPAM films were performed, and most of them were related to end-grafted PNIPAM [68–70]. In chains with one chain end-grafted to the solid support, a reduced ability to swell was found; however, a similar behavior to the PMDEGA film response was observed for poly(*N*-isopropylacrylamide) end-capped with *n*-butyltrithiocarbonate (nbc-PNIPAM) spin-coated onto solid supports [16]. The thinner the nbc-PNIPAM films were, the stronger was the response to swelling in saturated water vapor atmosphere. However, in nbc-PNIPAM a swelling of up to a factor of 6.5 as compared with the dry film was observed [16], whereas for PMDEGA the maximal swelling factor is 1.63. Thus, a 10.5 nm thick nbc-

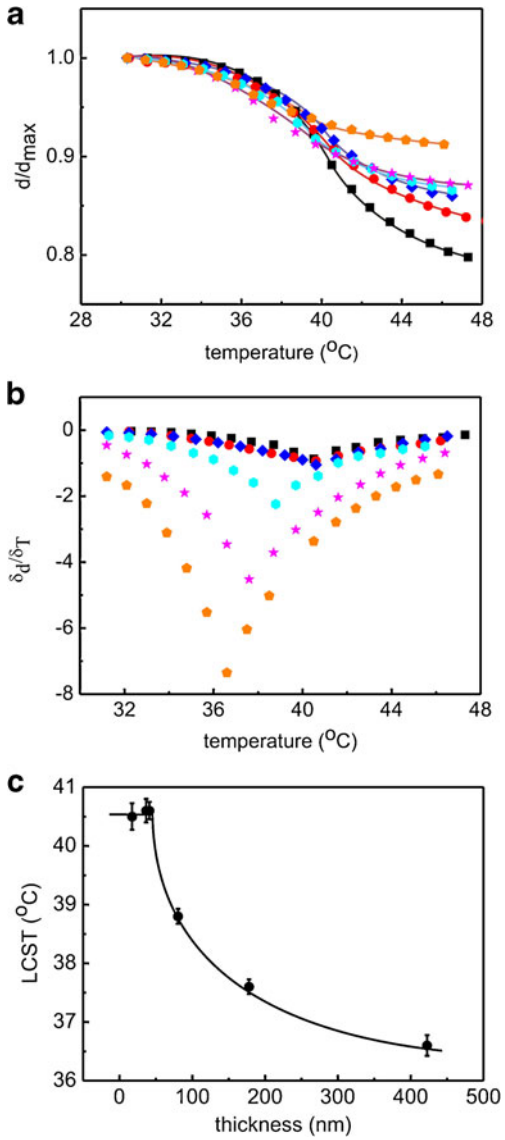

Fig. 12 **a** Temperature-dependent changes of the film thickness measured for PMDEGA films exposed to sodium chloride solution with concentration (0.045 g/mL). The film thickness varies from 17.4 (*squares*), 36.5 (*circles*), 41.1 (*rhombs*), 80.3 (*hexagons*), 178 (*stars*), to 422.6 nm (*pentagons*). The *solid lines* are guides to the eye. **b** Corresponding first derivatives of these data. **c** Thickness-dependent change of transition temperature measured for PMDEGA films (*dots*). The *solid line* is a guide to the eye

PNIPAM film responded by a more than 50% change of its thickness in the shrinkage [16], illustrating the much stronger response of nbc-PNIPAM as compared with PMDEGA. Therefore, differences in the observed swelling between nbc-PNIPAM and PMDEGA may result from the collapsed chain conformation, which, in the dry film, is due to the applied spin-coating technique. In combination with the hydrophilic substrate surface, which favors the PNIPAM or PMDEGA segments as well as water, the swelling might be increased by a type of entropic spring change in the conformation. The weaker response of the PMDEGA films is accompanied with a stronger shift in the transition temperature as compared with the nbc-PNIPAM. Therefore, nbc-PNIPAM and PMDEGA show an all-over similar behavior in thin films, but differ in the details due to the differences in the monomers and the resulting hydrogen bonding.

Very recently, in the case of nbc-PNIPAM films, it was shown that, with decreasing film thickness, the free volume increases [71]. As a consequence, it is the free volume which rules the maximum swelling capability of the nbc-PNIPAM films, and one might expect that the same is valid for the PMDEGA films probed in the present investigation.

Conclusions

Thin and homogeneous PMDEGA homopolymer hydrogel films on base-cleaned Si surfaces can be produced by spin-coating from 1,4-dioxane solution. Thus, solution and thin film behavior can be compared. The structural changes upon a thermally induced transition of the LCST-type from the swollen to a collapsed state in an aqueous solution and in thin films are probed. Though the thermal response of PMDEGA shares some similarities with the well-investigated PNIPAM, important differences were found. On the one hand, the absolute value of the LSCT is increased as compared with PNIPAM, being in the 45 °C to 38 °C range. This value is slightly above (instead of slightly below) body temperature which might offer certain advantages for biomedical applications.

Similar to the observations in PNIPAM, the PTT of thin PMDEGA hydrogel films is film-thickness-dependent. With increasing film thickness, the PTT decreases by 4 °C in good agreement with the observations for PNIPAM thin films on identical surfaces. However, all these thin films are non-bulk films and thus the PTT can be influenced by the interaction with the substrate. In the investigated range of film thickness (up to 422 nm), the bulk hydrogel behavior is not reached.

Concerning the width of the transition from a swollen to a collapsed state, PMDEGA differs from PNIPAM in that its transition is broader. Therefore, switching of PMDEGA solutions and thin films will require slightly larger changes in the temperature in comparison with PNIPAM. Moreover, the response is not that strong in PMDEGA films, meaning that the changes in film thickness are smaller as compared with PNIPAM films. Noteworthy is that, already after 1 day of storage under ambient conditions, an onset of de-wetting occurred. Although full film rupture into isolated droplets of PMDEGA did not happen, the films became heterogeneous.

Because preparation of the PMDEGA films out of 1,4-dioxane solution was done at ambient conditions already, even the freshly prepared films contain an unknown amount of water. Therefore, films denoted as "dry" are in reality

still slightly swollen. This might explain why PMDEGA films showed much less swelling as compared with PNIPAM films. All swelling experiments started with slightly swollen films already, whereas PNIPAM films absorb less water from the surrounding atmosphere and stay drier if prepared out of an organic solvent. Therefore, the affinity to water is higher for PMDEGA than for PNIPAM.

Acknowledgments We thank S. Beuermann (Universität Potsdam) for access to SEC equipment. We thank V. Körstgens, D. Magerl, A. Nathan, M. Rawolle, and M.A. Ruderer for the support during the BW4 experiments. Financial support by DFG in the priority program SPP1259 (PA771/4, LA611/7 and MU1487/8) is gratefully acknowledged.

References

1. Schild HG (1992) Prog Polym Sci 17:163
2. Lin S-Y, Chen K-S, Chu L-R (1999) Polymer 40:2619
3. Percot A, Zhu XX, Lafleur M (2000) J Polym Sci, Polym Phys 38:907
4. Katsumoto Y, Tanaka T, Sato H, Ozaki Y (2002) J Phys Chem A 106:3429
5. Koga T, Tanaka F, Motokawa R, Koizumi S, Winnik FM (2008) Macromolecules 41:9413
6. Troll K, Kulkarni A, Wang W, Darko C, Bivigou Koumba AM, Laschewsky A, Müller-Buschbaum P, Papadakis CM (2008) Colloid Polym Sci 286:1079 and Erratum (2011)
7. Sun S, Hu J, Tang H, Wu P (2010) J Phys Chem B 114:9761
8. Cho EC, Lee J, Cho K (2003) Macromolecules 36:9929
9. Hirokawa Y, Tanaka T, Matsuo ES (1984) J Chem Phys 81:6379
10. Housni A, Narain R (2007) Eur Polym J 43:4344
11. Shibayama M, Tanaka T, Han CC (1992) J Chem Phys 97:6829
12. Sato E, Tanaka T (1988) J Chem Phys 89:1695
13. Li Y, Tanaka T (1989) J Chem Phys 90:5161
14. Kim J-H, Ballauff M (1999) Colloid Polym Sci 277:1210
15. Nykänen A, Nuopponen M, Laukkanen A, Hirvonen S-P, Rytelä M, Turunen O, Tenhu H, Mezzenga R, Ikkala O, Ruokolainen J (2007) Macromolecules 40:5827
16. Wang W, Troll K, Kaune G, Metwalli E, Ruderer M, Skrabania K, Laschewsky A, Roth SV, Papadakis CM, Müller-Buschbaum P (2008) Macromolecules 41:3209
17. Wang W, Metwalli E, Perlich J, Papadakis CM, Cubitt R, Müller-Buschbaum P (2009) Macromolecules 42:9041
18. Wang W, Kaune G, Perlich J, Papadakis CM, Bivigou Koumba AM, Laschewsky A, Schlage K, Röhlsberger R, Roth SV, Cubitt R, Müller-Buschbaum P (2010) Macromolecules 43:2444
19. Tokarev I, Minko S (2009) Soft Matter 5:511
20. Cao Z, Du B, Chen T, Li H, Xu J, Fan Z (2008) Langmuir 24:5543
21. Nayak S, Debord SB, Lyon LA (2003) Langmuir 19:7374
22. Serpe MJ, Lyon LA (2004) Chem Mater 16:4373
23. Cheng X, Canavan HE, Stein MJ, Hull JR, Kweskin SJ, Wagner MS, Somorjai GA, Castner DG, Ratner BD (2005) Langmuir 21:7833
24. Harmon ME, Kuckling D, Frank CW (2003) Langmuir 19:10660
25. Jagur-Grodzinski J (2010) Polym Adv Technol 21:27
26. Cooperstein MA, Canavan HE (2010) Langmuir 26:7695
27. Rana D, Matsuura T (2010) Chem Rev 110:2448
28. Akdemir Ö, Badi N, Pfeifer S, Zarafshani Z, Laschewsky A, Wischerhoff E, Lutz J-F (2009) ACS Symp Ser 1023:189
29. Hua F, Jiang X, Li D, Zhao B (2006) J Polym Sci, A, Polym Chem 44:2454
30. Iwata H, Oodate M, Uyama Y, Amemiya H, Ikada Y (1991) J Membr Sci 55:119
31. Ying L, Kang ET, Neoh KG, Kato K, Iwata H (2003) Macromol Mater Eng 288:11
32. Yim H, Kent MS, Huber DL, Satija S, Majewski J, Smith GS (2003) Macromolecules 36:5244
33. Yim H, Kent MS, Mendez S, Lopez GP, Satija S, Seo Y (2006) Macromolecules 39:3420
34. Miyamae T, Akiyama H, Yoshida M, Tamaoki N (2007) Macromolecules 40:4601
35. Ishida N, Biggs S (2007) Macromolecules 40:9045
36. Hirata I, Okazaki M, Iwata H (2004) Polymer 45:5569
37. Bivigou Koumba AM, Kristen J, Laschewsky A, Müller-Buschbaum P, Papadakis CM (2009) Macromol Chem Phys 210:565
38. Müller-Buschbaum P (2003) Eur Phys J E 12:443
39. Kline SR (2006) J Appl Crystallogr 39:895
40. Horkay F, Hecht AM, Mallam S, Geissler E, Rennie AR (1991) Macromolecules 24:2896
41. Braun C, Parratt32, Version 1.6, HMI Berlin (2002)
42. Parratt LG (1954) Phys Rev 95:359
43. Roth SV, Döhrmann R, Dommach M, Kuhlmann M, Kröger I, Gehrke R, Walter H, Schroer C, Lengeler B, Müller-Buschbaum P (2006) Rev Sci Instrum 77:085106
44. Müller-Buschbaum P, Bauer E, Pfister S, Roth SV, Burghammer M, Riekel C, David C, Thiele U (2006) Europhys Lett 73:35
45. Yoneda Y (1963) Phys Rev 131:2010
46. Salditt T, Metzer TH, Peisel J, Reinker B, Moske M, Samwer K (1995) Europhys Lett 32:331
47. Müller-Buschbaum P, Vanhoorne P, Scheumann V, Stamm M (1997) Europhys Lett 40:655
48. Müller-Buschbaum P (2003) Anal Bioanal Chem 376:3
49. Renaud G, Lazzari R, Leroy D (2009) Surf Sci Rep 64:255
50. Garnweitner G, Smarsly B, Assink R, Dunphy DR, Scullin C, Brinker CJ (2004) Langmuir 20:9811
51. Barbey R, Lavanant L, Paripovic D, Schwer N, Sugnaux C, Tugulu S, Klok H-A (2009) Chem Rev 109:5437
52. Xu W, Siow KS, Gao Z, Lee SY (1998) Chem Mater 10:1951
53. Mertoglu M, Laschewsky A, Skrabania K, Wieland C (2005) Macromolecules 38:3601
54. Gruendling T, Pickford R, Guilhaus M, Barner-Kowollik C (2008) J Polym Sci, A, Polym Chem 46:7447
55. Päch M, Zehm D, Lange M, Dambowsky I, Weiss J, Laschewsky A (2010) J Am Chem Soc 132:8757
56. Furyk S, Zhang Y, Ortiz-Acosta D, Cremer PS, Bergbreiter DE (2006) J Polym Sci, A, Polym Chem 44:1492
57. Skrabania K, Kristen J, Laschewsky A, Akdemir Ö, Hoth A, Lutz J-F (2007) Langmuir 23:84
58. Simon JH, Geraldine GD, Chert-Tsun Y, Elodie I, Nicholas JH, Tim HR (2008) J Polym Sci, A, Polym Chem 46:7739
59. Aseyev V, Tenhu H, Winnik F (2011) Adv Polym Sci. doi:10.1007/12_2010_57,onlinefirst
60. Kratky O, Laggner P (1987) Encycl Phys Sci Technol 14:693
61. Okada Y, Tanaka F (2005) Macromolecules 38:4465
62. Schubert DW, Dunkel T (2003) Mat Res Innovat 7:314
63. Müller-Buschbaum P (2003) J Phys Condens Matter 15:R1549
64. Fryer DS, Nealey PF, De Pablo JJ (2000) Macromolecules 33:6439
65. Daillant J, Belorgey O (1992) J Chem Phys 97:5824
66. Holy V, Baumbach T (1994) Phys Rev B 49:10668
67. Müller-Buschbaum P, Stamm M (1998) Macromolecules 31:3686
68. Yan Q, Hoffman AS (1995) Polymer 36:887
69. Kaneko Y, Nakamura S, Sakai K, Aoyagi T, Kikuchi A, Sakurai Y, Okano T (1998) Macromolecules 31:6099
70. Kaholek M, Lee W-K, Ahn S-J, Ma H, Caster KC, LaMattina B, Zauscher S (2004) Chem Mater 16:3688
71. Harms S, Rätzke K, Faupel F, Egger W, Ravelli L, Laschewsky A, Wang W, Müller-Buschbaum P (2010) Macromol Rapid Commun 31:1364